ACS APPLIED MATERIALS & INTERFACES

Research Article

www.acsami.org

Fabrication of SiO_2/TiO_2 Double-Shelled Hollow Nanospheres with Controllable Size via Sol–Gel Reaction and Sonication-Mediated Etching

Jungsup Lee, Sun Hye Hwang, Juyoung Yun, and Jyongsik Jang*

School of Chemical and Biological Engineering, Seoul National University, 599 Gwanangno, Gwanakgu, Seoul 151-742, Korea

Supporting Information

ABSTRACT: Size-controllable double-shell SiO_2/TiO_2 hollow nanoparticles (DS HNPs) were fabricated using a simple sol–gel reaction and sonication-mediated etching. The size of the DS HNPs was controlled using SiO_2 core templates of various sizes. Moreover, monodisperse DS HNPs were produced on a large scale (10 g per 1 batch) using the sol–gel method. The surface area and porosity of intrashell and inner-cavity pores were measured by Brunauer–Emmett–Teller analysis. As a result, 240 nm DS HNPs (240 DS HNPs) exhibited the highest surface area of 497 $m^2\ g^{-1}$ and a high porosity. Additionally, DS HNPs showed excellent light-scattering ability as a scattering layer in dye-sensitized solar cells due to their structural properties, such as a composite, double-shell, hollow structure, as well as intrashell and inner cavity pores. The DSSCs incorporating 240 DS HNPs demonstrated an 18.3% enhanced power conversion efficiency (PCE) compared to TiO_2 nanoparticles.

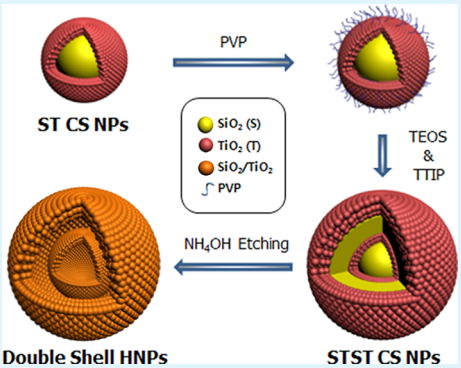

KEYWORDS: *double-shell hollow nanoparticles, porous nanoparticle, sol–gel method, light scattering, dye-sensitized solar cell*

INTRODUCTION

Hollow nanoparticles (HNPs) are considered to be a promising structure for drug delivery systems,[1−3] catalysts,[4] chemical and biological sensors,[5,6] and solar cells.[7,8] The inner cavity of the hollow particles offers a large volume for transport of drugs, DNA, and cosmetics, which is essential for drug delivery systems.[1−3] HNPs exhibit high catalytic and sensor activities, because their inner- and outer-shell surfaces facilitate contact with reactant molecules.[7] The light-scattering effect can be enhanced by increasing the difference between the refractive indices of the empty inner cavity and solid shell of HNPs.[2,9−11] Although HNPs demonstrate these advantages, design of an optimized structure for specific application fields to further enhance their performance remains challenging.

To enhance the advantages of the hollow structure, multishell HNPs have recently attracted interest due to their outstanding light-scattering effect and large surface area. The multishell structure provides enhanced light scattering by repeated reflection and scattering events between the inner and outer shells.[12] Moreover, the active surface area is larger, compared with that of a single shell, due to the surface area of the additional inner shells.

In recent years, much research has aimed to develop a method of fabricating multishell HNPs to improve their performance in various applications.[5,13−16] Pan et al. reported use of hydrothermal synthesis to fabricate a double-shell $LiMn_2O_4$ hollow sphere, in an attempt to optimize the performance of lithium ion batteries.[17] Compared with single-shell HNPs (SS HNPs), the improved performance of the battery with the double-shell configuration was attributed to an increase in the contact area between the electrode and electrolyte created by the hollow interior and gap between the shells. Zhang et al. used the hydrothermal method to produce microscale ZnO multishell hollow spheres that exhibited marked sensitivity for detection of toluene, due to their large surface area.[18] Wu et al. hydrothermally synthesized double shell TiO_2 hollow spheres, which exhibited an enhanced light-scattering ability for dye-sensitized solar cell (DSSC) applications.[19] Previous approaches to manufacturing multishell hollow structures involved mainly hydrothermal reactions using an autoclave, which limited the ability to control the size and aggregation of particles due to high reaction temperature. Thus, there is a growing demand for methods of fabricating multishell hollow particles at the nanoscale, with high surface area and monodispersity.

Herein, we suggest a simple fabrication method for SiO_2/TiO_2 double-shell HNPs (DS HNPs) based on the sol–gel reaction and sonication-mediated etching. In this work, the particle size can be easily controlled over the range from 120 to 240 nm using silica core templates of various sizes. The pore distribution and surface area of DS HNPs were investigated using nitrogen adsorption/desorption isotherms. DS HNPs, 240 nm in size, exhibited a high surface area of 497 $m^2\ g^{-1}$ because of the presence of pores within the inner and outer

Received: June 20, 2014
Accepted: August 22, 2014
Published: August 22, 2014

shells. The double-shell structure of DS HNPs exhibited enhanced light-scattering compared with SS HNPs via multiple scattering events between the inner and outer shells. Additionally, the photovoltaic performance of the DS HNPs, as a light-scattering material, was estimated in the anode electrode of DSSCs.

EXPERIMENTAL SECTION

Materials. Titanium(IV) isopropoxide (TTIP, 97%), tetraethyl orthosilicate (TEOS, 98%), and polyvinylpyrrolidone (PVP, MW = 10 000 000) were obtained from Aldrich Chemical Co. (St. Louis, MO). Ammonia solution (28−30%) was purchased from Samchun Chemical Co. TiO_2 NPs (Ti-nanoxide T/SP) and *cis*-disothiocyanato-bis(2,20-bipyridyl-4,40-dicarboxylato)ruthenium-(II) bis(tetrabutylammonium) (N-719), and an iodide-based redox electrolyte (AN50) were purchased from Solaronix (Aubonne, Switzerland). FTO glass (15 Ω cm^{-2}, thickness of 2.2 mm) was obtained from Pilkington (Toledo, USA)

Synthesis of Double-Shell SiO_2/TiO_2 Hollow Nanoparticles (DS HNPs). Colloidal suspension (80 mL) containing 0.75 g of silica nanoparticles were fabricated using the Stöber method.[20] Titanium-(IV) isopropoxide (TTIP) (3.6 mL) was added to a colloidal solution of silica nanoparticles−mixed with 18 mL of ethanol, and 6 mL of acetonitrile. The TTIP-dropped colloidal solution of SiO_2 nanoparticles reacted at 4 °C for 6 h to obtain SiO_2/TiO_2 core/shell nanoparticles (ST CSNPs) via the sol−gel reaction. The prepared ST CSNPs were obtained by centrifugation at 12,000 rpm for 20 min and then redispersed in 80 mL of deionized water with the same amount of PVP. The solution containing well-dispersed ST CSNPs and PVP was stirred for 12 h to allow for the adsorption of PVP on the surface of the ST CSNPs. The PVP adsorbed ST CSNPs were then centrifuged and redipersed in 158 mL of ethanol. The solution was mixed with 1.4 mL of deionized water and 2 mL of 0.1 M ammonia solution. Tetraethyl orthosilicate (TEOS) (5.8 mL) was added to the colloidal solution and stirred at 38 °C for 4 h to coat the ST CSNP surface with SiO_2. A solution of 5.8 mL TTIP, 9 mL ethanol, and 3 mL acetonitrile was added to the above colloidal solution. The TTIP-dropped colloidal solution of STS CSNPs reacted at 4 °C for 6 h to produce $SiO_2/TiO_2/SiO_2/TiO_2$ core/shell nanoparticles (STST CSNPs) via the sol−gel reaction. The hollow structure was fabricated by redeposition in a 0.1 M ammonia solution and sonication-mediated etching for 6 h. The final DS HNP product was obtained by centrifugation at 12 000 rpm for 10 min and washing the solution with ethanol twice. The evolution mechanism for the conversion of ST CSNPs to DS HNPs is described in a previous study.[13]

Preparation of a DS HNP Paste as a Scattering Layer. Pastes of SS HNPs and DS HNPs, 120, 150, 180, and 240 nm in size, were prepared by incorporating samples of the mixture of lauric acid, ethyl cellulose, and terpineol containing TiO_2 NPs (size = 15−20 nm). The SS HNPs or DS HNPs were added to the terpineol-based paste (HNPs, 15−25 wt %). The anode film was composed of a 7.5-μm-thick underlayer containing only TiO_2 NPs (size, 15−20 nm) and a 2.5-μm-thick overlayer composed of the prepared paste mixture of TiO_2 NPs and SS HNPs or DS HNPs.

Assembly of Dye-Sensitized Solar Cells (DSSCs). The TiO_2 film with a double-layered structure was composed of a TiO_2 NP (Solaronix, Ti-Nanoxide T/sp) underlayer and an SS HNP or DS HNP overlayer. Fluorine-doped tin oxide (FTO) glass substrates were cleaned by successive sonication in deionized water, acetone, and 2-propanol for 60 min each, and then treated with oxygen plasma for 30 s. The FTO glass substrates were pretreated with 40 mM $TiCl_4$ solution and heated at 450 °C for 30 min. A photoanode was prepared by applying a TiO_2 NPs underlayer and Ag-decorated HNPs with a SiO_2 overlayer to the FTO substrate using a screen-printing technique. The photo anodes were sintered at 450 °C for 30 min, and then treated with $TiCl_4$ and sintered again as above. The resulting TiO_2 films were immersed in absolute ethanol containing 5×10^{-4} M of N719 and kept at room temperature for 24 h. Pt counter electrodes were added to the FTO glass using a 5 mM H_2PtCl_6 solution, followed by heating at 400 °C for 30 min in air. The electrolyte used in the sealed cell was an I^-/I_3^- redox couple containing 0.60 M BMII, 0.1 M LiI, 0.05 M I_2, and 0.5 M *t*-butylpyridine in acetonitrile.

Instrument. The morphology of the DS HNPs was investigated using field-emission scanning electron microscopy (FE-SEM) (6700; JEOL, Tokyo, Japan) and transmission electron microscopy (TEM) (JEM-200CX; JEOL). The scanning TEM/energy-dispersive X-ray (STEM-EDX) data were obtained using a Technai F20 (FEI) spectrometer. Electron energy loss spectroscopy (EELS) mapping of the DS HNPs was performed using a Carl Zeiss LIBRA 200 FE microscope. Brunauer−Emmett−Teller (BET) surface areas of HNPs were determined using a Micromeritics analyzer (ASAP 2000; Micromeritics Co., Norcross, GA). A Lambda 35 spectrophotometer (PerkinElmer) was used for ultraviolet−visible (UV−vis) diffuse reflectance spectroscopy (DRS). The photocurrent density−voltage ($J-V$) characteristics of the assembled DSSCs were evaluated using a 500-W xenon lamp (XIL model 05A50KS source units). The incident photon-to-current efficiency (IPCE; PV Measurements, Inc., Boulder, CO) was measured over the range of 300−800 nm under the global AM 1.5 solar emission spectrum.

RESULTS AND DISCUSSION

Scheme 1 illustrates the fabrication procedure of the DS HNPs. First, we synthesized silica NPs for the core template via the Stöber method. By sol−gel reaction, a TiO_2 shell is formed on the SiO_2 core by adding TTIP to the colloidal solution of SiO_2 NPs. The prepared SiO_2/TiO_2 core/shell nanoparticles (ST CSNPs) were coated with PVP to improve the affinity of the TiO_2 shell to the SiO_2 precursor. PVP adsorbed to the TiO_2 shell through interactions between the negatively charged carbonyl group within PVP and the hydroxyl groups of the oxide surfaces.[21] The ST CSNPs treated with PVP were then coated with a SiO_2 layer by adding TEOS, resulting in $SiO_2/TiO_2/SiO_2$ core/shell nanoparticles (STS CSNPs). Finally, $SiO_2/TiO_2/SiO_2/TiO_2$ core/shell nanoparticles (STST CSNPs) were formed via a sol−gel reaction by dropping TTIP into the colloidal solution of STS CSNPs. To obtain DS HNPs, prepared STST CSNPs were etched with NH_4OH under sonication.

Scheme 1. Schematic Illustration of the Formation Procedure for Double-Shell SiO_2/TiO_2 Hollow Nanoparticles (DS HNPs) with a Highly Porous Structure via Polyvinylpyrrolidone (PVP) Adsorption on TiO_2, the Sol−Gel Reaction, and an Etching Process

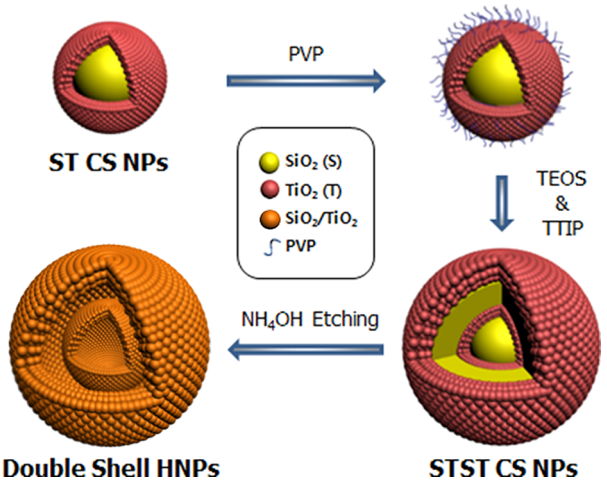

Figure 1 shows a TEM image of the size-controlled DS HNPs. The size of the DS HNPs was easily controlled by

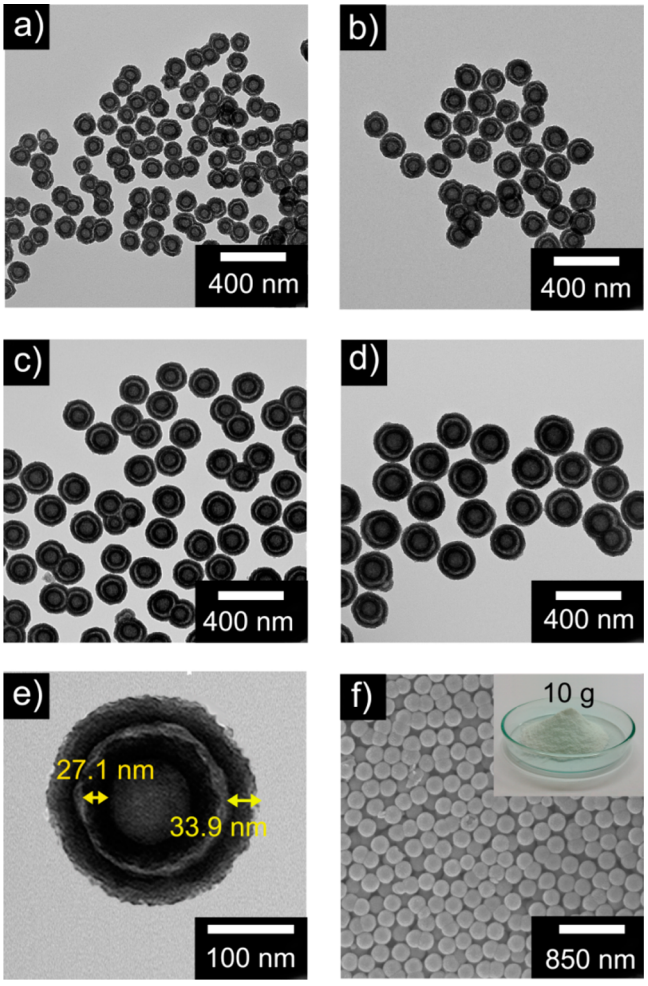

Figure 1. Transmission electron microscopy (TEM) images of double-shelled hollow nanoparticles (DS HNPs) of various size of (a) 120, (b) 150, (c) 180, and (d) 240 nm. High-magnification TEM image of e) 240 nm DS HNPs (240 DS HNPs). Scanning electron microscopy (SEM) image of (f) 240 DS HNPs. Inset: Amount of 240 DS HNPs fabricated in one batch; 10 g.

introducing different sized silica core templates. Using a silica core template of 40, 60, 80, and 120 nm, the size of the DS HNPs varied by 120, 150, 180, and 240 nm (Figure 1a–c). Table 1 shows the shell thicknesses and diameters of DS HNPs

Table 1. Size and Inner/Outer Shell Thicknesses of the Double-Shell Hollow Nanoparticles (DS HNPs)

sample	inner shell thickness (nm)	outer shell thickness (nm)	inner diameter (nm)	outer diameter (nm)
DS 120	10.8 ± 5	13.5 ± 5	81.2 ± 5	122.0 ± 5
DS 150	13.5 ± 5	16.9 ± 5	101.6 ± 5	149.1 ± 5
DS 180	19.9 ± 5	24.9 ± 5	124.4 ± 5	179.3 ± 5
DS 240	27.1 ± 5	33.9 ± 5	152.5 ± 5	237.3 ± 5

of different sizes. The thickness of the shell had a tendency to increase as the size of the DS HNPs increased. We confirmed DS HNPs with a size of 240 nm (240 DS HNPs) fabricated with inner and outer shell thicknesses of 27.1 and 33.9 nm, respectively; the shells possessed porosity and roughness (Figure 1e). Additionally, by increasing the amount of TEOS during the formation of the second SiO_2 layer, the outer shell thickness of the DS HNPs could be doubled (Supporting Information Figure S2). Not only the shell thickness of the double shell, but also that of the single shell SiO_2/TiO_2 hollow nanoparticles (SS HNPs) could be controlled. By adjusting the size of the silica core template and the amount of dropped TTIP, SS HNPs with a thick shell were readily fabricated (Supporting Information Figure S3). Figure 1f shows a FE-SEM image of 240 DS HNPs.

The atomic distribution of the Si and Ti regions in the DS HNPs was confirmed using STEM-EDX, as shown in Figure 2.

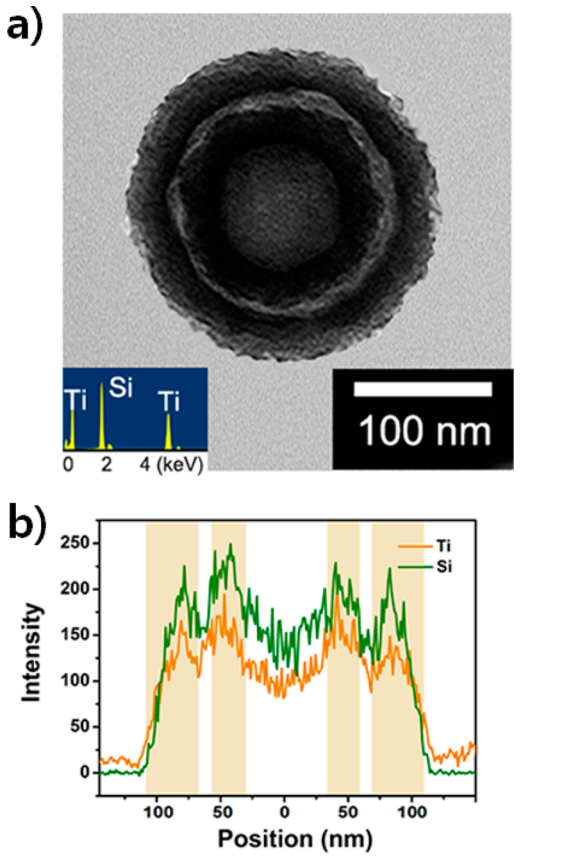

Figure 2. (a) Magnified TEM image (inset shows atomic ratio of Si = 55.54 and Ti = 44.46) and (b) scanning TEM/energy dispersive X-ray (STEM-EDX) line scan of 240 nm DS HNPs.

The measured atomic ratio of Ti to Si was 0.8 according to STEM-EDX, revealing that a considerable amount of SiO_2 was present in the DS HNPs after the etching process. Figure 2b shows the line scan of DS HNPs, which indicated the presence of both Si and Ti atoms in the inner and outer shells. These data confirmed that the hollow-structured double shells were composed of both Si and Ti atoms.

To analyze the porosity of DS HNPs, nitrogen adsorption and desorption isotherms were measured for 120, 150, 180, and 240 DS HNPs. Figure 3 shows that isotherms of the DS HNPs are type IV according to Brunauer–Deming–Deming–Teller (BDDT) classification, which indicates the mesoporous structure of DS HNPs. Also, DS HNPs displayed type H2 hysteresis loops because of disordered porous structures. The desorption of nitrogen, with a relative pressure ranging from 1.0 to 0.5, was delayed, compared with adsorption for the same relative pressure range. The delayed desorption was attributed to condensated nitrogen in the intrashell pores of the DS

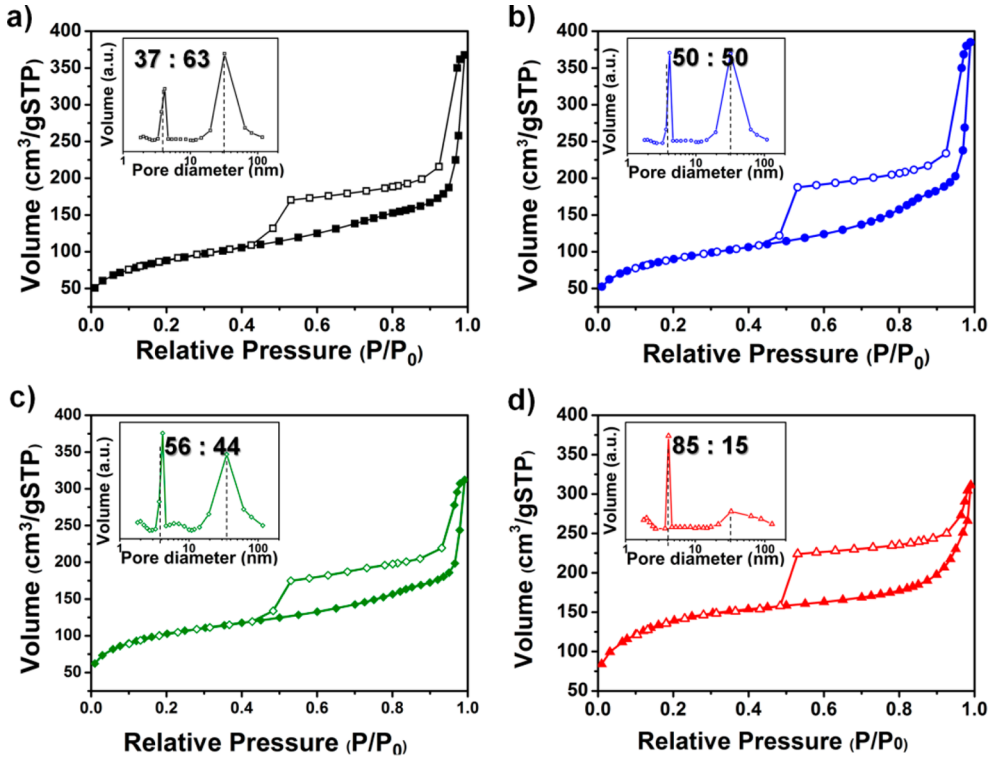

Figure 3. Nitrogen adsorption and desorption isotherms of (a) 120 (black), (b) 150 (blue), (c) 180 (green). and (d) 240 nm (red) DS HNPs. The pore volume distribution of the DS HNPs was derived from the desorption isotherms.

HNPs, which blocked the evaporation of nitrogen in the inner cavity. The desorbed volume at a relative pressure of 0.95−1 corresponded to the volume of nitrogen which had adsorbed to the outer-shell surface of the DS HNPs. Figures 3a and b, corresponding to 120 and 150 DS HNPs respectively, show an almost identical amount of desorbed nitrogen. However, the amount of desorbed nitrogen decreased sharply with increasing size of the DS HNPs. These results, taken together, indicated that the outer-shell surface area of the 240 DS HNPs was smallest among the DS HNPs; thus, that of the 120 DS HNPs was largest. Moreover, this result was in good agreement with the TEM image (Figure 1).

To gain insight into the pore structure of DS HNPs, the surface area of the intrashell pores (A_{ISP}) and the shell without pores within the intrashell (A_{shell}) of DS HNPs was calculated using the formula[22]

$$A_{shell} = 3V_{SiO_2/TiO_2}(R^2 + r^2)/(R^3 - r^3)$$

$$A_{ISP} = A_{BET} - A_{shell}$$

Here, $V_{SiO_2/TiO_2} = 1/\rho_{SiO_2/TiO_2} = 0.333$ cm^3 g^{-1} represents the specific volume of the TiO_2/SiO_2 composites. R and r are the outer and inner radii of the shell, and ρ_{SiO_2/TiO_2} is the density of the SiO_2/TiO_2 composite. The calculated values for A_{shell} and A_{ISP} are listed given in Table 2. The A_{shell} decreased from 112 to 45 m^2 g^{-1} as the DS HNP size increased from 120 to 240 nm, while A_{BET} increased from 317 to 497 m^2 g^{-1}. Interestingly, the 240 DS HNP showed the largest A_{BET}, despite having the smallest A_{shell}. The number of intrapores within the shell may have increased with increasing size of the DS HNPs because of the thicker shell. Therefore, 240 DS HNPs exhibited the largest surface area due to the large number of intrashell pores. The pore distribution of DS HNPs (inset to Figures 3a−d) supports this assumption. The DS HNPs were composed mainly of small pores (size = 4.1 ± 0.5 nm) and large pores (size = 32 ± 3 nm) within the intrashell and large inner cavity. The ratio of small pores to large pores increased linearly, reaching 85:15 for the 240 DS HNPs, and the ratio of intrashell pores increased with increasing DS HNP size. Thus, intrashell pores predominated in terms of contribution to the surface area of DS HNPs and 240 DS HNPs exhibited the highest surface area.

Table 2. Brunauer−Emmett−Teller (BET) Analysis of the Total Surface Area (A_{BET}), Surface Area of the Intrashell Pores (A_{ISP}), and the Shell without Pores within the Intrashell (A_{shell}) of DS HNPs (where $A_{ISP} = A_{BET} - A_{shell}$)

sample	A_{BET} (m^2 g^{-1})	A_{shell} (m^2 g^{-1})	A_{ISP} (m^2 g^{-1})
120 DS	317	112	205
150 DS	351	89.0	262
180 DS	366	63.0	303
240 DS	497	45.0	452
240 SS	482	14.0	468

Diffuse reflectance spectra (DRS) were obtained to compare the light-scattering effect of fabricated DS HNPs with SS HNPs. DRS for 120, 150, and 180 DS HNPs were additionally presented. In Figure 4a, the diffuse reflectance tended to increase with increasing DS HNPs size in the range of 120−240 DS HNPs. Among the fabricated DS HNPs, 240 DS HNPs showed the highest reflectance because of the enhanced light scattering effect coming from the larger size of particles.[23] There is a probability that light-scattering of DS HNPs might increase with larger size than 240 nm, as there exists unique diameter that shows the high scattering efficiency.[24] The unique diameter is generally the similar size as that of the visible light's wavelength, sized 390−700 nm.[25] However, further research on size-dependence of light-scattering will be included in later

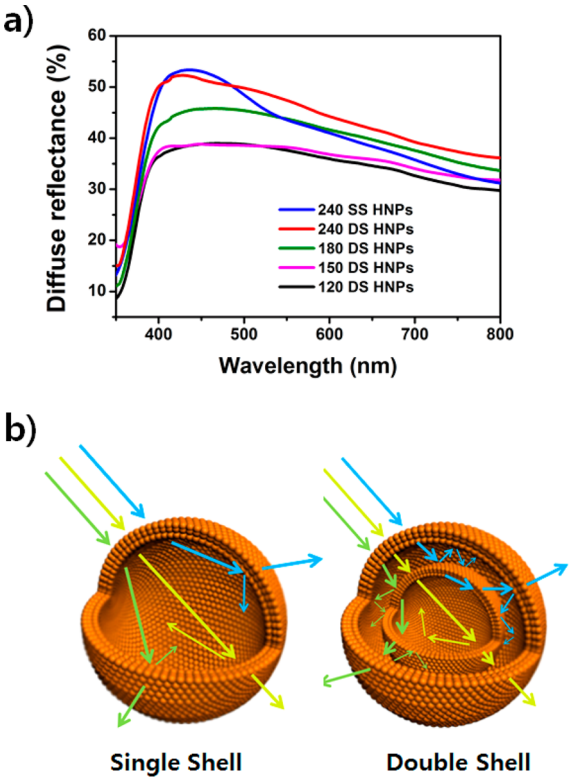

Figure 4. (a) Diffuse reflectance spectra for DS HNPs of different sizes and 240 single-shell HNPs (SS HNPs). (b) Schematic illustration of the light scattering effect within SS HNPs and DS HNPs.

studies as it is slightly out of our primary focus. 240 DS HNPs exhibited higher diffuse-reflectance than 240 SS HNPs. The double-shell structures of DS HNPs within a working electrode exhibit increased light scattering compared with SS HNPs due to the multiple scattering events that occur between the inner shell and outer shell (Figure 4b).[12,26,27] Further, DS HNPs composed of SiO_2 and TiO_2 form a composite structure. The refractive indices for anatase TiO_2 NPs and SiO_2 NPs are 2.40 and 1.47, respectively; this significant difference between the two indices enhances the light-scattering efficiency.[28] Moreover, the numerous pores on the shell surfaces of the DS HNPs contribute to the light-scattering effect, in particular, optical Rayleigh scattering.[29] This effect is further enhanced by the hollow structure of the DS HNPs (i.e., the inner cavity and gap between shells) increasing light-scattering. Thus, the hollow structure lengthens the path length of the incident light by increasing the number of light-scattering events between shells and within the intrashell pores.[12,26]

To investigate how the light-scattering affects the performance of DSSCs, prepared DS HNPs were introduced as scattering layers. By employing DS HNPs as scattering layer, we could analyze how light-scattering ability of DS HNPs affect increase in PCE, apart from influences of dye absorption or electrical conductivity. The TiO_2 film in the working electrode was composed of a 7.5-μm-thick TiO_2 NPs (size = 15−20 nm) underlayer and a 2.5-μm-thick overlayer composed of a prepared mixture paste of TiO_2 NPs and 240 SS HNPs or 240 DS HNPs, with pristine TiO_2 NPs introduced as a control. Supporting Information Figure S1 shows the dependence of current density (J_{sc}) on the concentration of 240 DS HNPs. Same experiments were done over 5 times, and average PCE and standard deviation were calculated for error analysis (Supporting Information Table S1). Figure 5 shows one of the data acquired. The DSSCs containing a DS HNP scattering

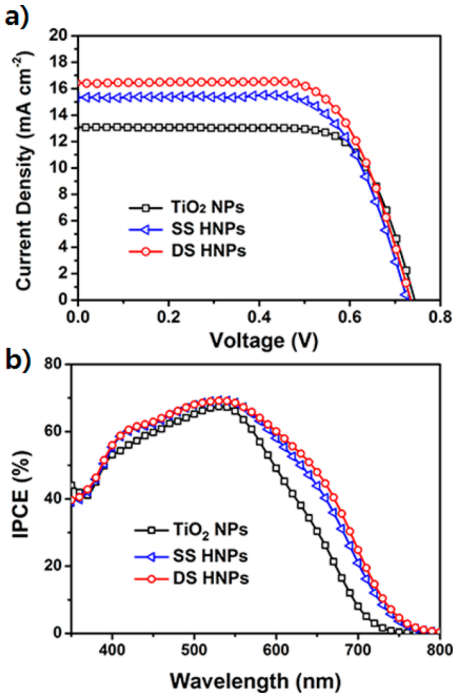

Figure 5. (a) Current density−voltage (J_{sc}−V) curves for TiO_2 NPs (size = 15−20 nm), SS HNPs (size = 240 nm), and DS HNPs (size = 240 nm) material-based dye-sensitized solar cells (DSSCs). (b) Incident photon-to-current efficiency (IPCE) of DSSCs.

layer (content = 22.5 wt %) showed a short-circuit current density (J_{sc}) value of 16.4 mA cm^{-2}; whereas the J_{sc} of DSSCs decreased significantly when the amount of 240 DS HNPs was greater than 22.5 wt %. The photogenerated electron cannot transfer through the DS HNPs because of its composite composition (i.e., amorphous SiO_2 and TiO_2 content). Thus, a large concentration of DS HNPs (>22.5 wt % 240 DS HNPs) inhibits electron transfer into the working electrode, significantly limiting the light scattering; this leads to a reduction in J_{sc}. Figure 5a displays the short-circuit current density−voltage (J_{sc}−V) curve of DSSCs with an anode film that incorporates TiO_2 NPs, SS HNPs, or DS HNPs. The performance parameters for the tested DSSCs are presented in Table 3. The J_{sc} value for TiO_2 NP, SS HNP, and DS HNP incorporated cells was 13.1, 15.3, and 16.4 mA cm^{-2}, respectively. Compared with TiO_2 NPs and SS HNPs, the J_{sc} values for anode films with DS HNPs were 25.2% and 7.2% higher, indicating the enhanced light scattering effect of DS HNPs; this effect was

Table 3. Summary of Photovoltaic Properties of TiO_2 NPs, SS HNPs, and DS HNPs-Based Dye-Sensitized Solar Cells (DSSCs)

sample[a]	J_{sc}[b] (mA cm^{-2})	V_{oc}[c] (V)	FF[d]	η[e] (%)
TiO_2 NPs	13.1	0.74	0.73	7.1
SS HNP	15.3	0.74	0.70	7.9
DS HNP	16.4	0.74	0.69	8.4

[a]Active area of the assembled DSSC samples is 0.16 cm^2. [b]Short-circuit current. [c]Open-circuit voltage. [d]Fill factor. [e]Power conversion efficiency.

attributed to their double-shell structure, as discussed earlier. This tendency was also revealed in the incident-photon-to-current efficiency (IPCE) spectra, shown in Figure 5b. DS HNPs and SS HNPs exhibited higher quantum efficiency (QE) than TiO_2 NPs, especially at the long wavelength region. This suggests that hollow structured materials display improved QE in the long wavelength region due to large adsorption of dye and high light scattering. Moreover, higher QE of DS HNPs compared to SS HNPs is attributed to additional dye loading and multi light-scattering, which are derived from the second shell.

CONCLUSION

In conclusion, DS HNPs were successfully fabricated via a sol−gel method and etching. The size and shell thickness of DS HNPs was easily controlled by varying the silica core size and the amount of dropped TTIP. The DS HNPs that were larger in size exhibited larger surface areas due to additional pores within the intrashells, with 240 DS HNPs being the largest. DS HNPs demonstrated enhanced light scattering through light confinement, optical Rayleigh scattering, and reflections induced by the composite structure, double-shell hollow structure, and intrashell and inner cavity pores. With such a high scattering ability, DSSCs using DS HNPs as a scattering layer exhibited a high power conversion efficiency of 8.4%, which is 18.3% and 6.3% higher than those of DSSCs using TiO_2 NPs (7.1%) and SS HNPs (7.9%). This novel fabrication process provides the means to design various multishelled hollow structures for drug delivery, photocatalysts, chemical and bio sensors, and DSSCs

ASSOCIATED CONTENT

Supporting Information

(1) Current density (J_{sc}) of the anode film as a function of DS HNP concentration (contents = 15−25 wt %) in the scattering layer, (2) TEM images of 120 nm double-shell hollow nanoparticles (DS HNPs) with a thickness of 10 and 20 nm and (3) single-shell HNPs (SS HNPs) 240 nm in size, and (4) average of power conversion efficiency (PCE) and standard deviation of all experiments held. This material is available free of charge via the Internet at http://pubs.acs.org.

AUTHOR INFORMATION

Corresponding Author

*E-mail: jsjang@plaza.snu.ac.kr.

Notes

The authors declare no competing financial interest.

ACKNOWLEDGMENTS

This work was supported by Global Frontier R&D Program on Center for Multiscale Energy System funded by the National Research Foundation under the Ministry of Education, Science and Technology, Korea (2011-0031573).

REFERENCES

(1) Lou, X. W.; Archer, L. A.; Yang, Z. Hollow Micro-/Nanostructures: Synthesis and Applications. *Adv. Mater.* **2008**, *20*, 3987−4019.

(2) Xie, Q.; Zhao, Y.; Chen, X.; Liu, H.; Evans, D. G.; Yang, W. Nanosheet-Based Titania Microspheres with Hollow Core-Shell Structure Encapsulating Horseradish Peroxidase for a Mediator-Free Biosensor. *Biomaterials* **2011**, *32*, 6588−6594.

(3) Zhu, Y.; Shi, J.; Shen, W.; Dong, X.; Feng, J.; Ruan, M.; Li, Y. Stimuli-Responsive Controlled Drug Release from a Hollow Mesoporous Silica Sphere/Polyelectrolyte Multilayer Core−Shell Structure. *Angew. Chem., Int. Ed.* **2005**, *44*, 5083−5087.

(4) Liang, H. P.; Zhang, H. M.; Hu, J. S.; Guo, Y. G.; Wan, L. J.; Bai, C. L. Pt Hollow Nanospheres: Facile Synthesis and Enhanced Electrocatalysts. *Angew. Chem., int. Ed.* **2004**, *43*, 1540−1543.

(5) Zhang, H.; Zhu, Q.; Zhang, Y.; Wang, Y.; Zhao, L.; Yu, B. One-Pot Synthesis and Hierarchical Assembly of Hollow Cu_2O Microspheres with Nanocrystals-Composed Porous Multishell and Their Gas-Sensing Properties. *Adv. Funct. Mater.* **2007**, *17*, 2766−2771.

(6) Guo, Z.; Seol, M. L.; Kim, M. S.; Ahn, J. H.; Choi, Y. K.; Liu, J. H.; Huang, X. J. Hollow CuO Nanospheres Uniformly Anchored on Porous Si Nanowires: Preparation and Their Potential Use as Electrochemical Sensors. *Nanoscale* **2012**, *4*, 7525−7531.

(7) Hwang, S. H.; Shin, D. H.; Yun, J.; Kim, C.; Choi, M.; Jang, J. SiO_2/TiO_2 Hollow Nanoparticles Decorated with Ag Nanoparticles: Enhanced Visible Light Absorption and Improved Light Scattering in Dye-Sensitized Solar Cells. *Chem.—Eur. J.* **2014**, *20*, 4439−4446.

(8) Koo, H. J.; Kim, Y. J.; Lee, Y. H.; Lee, W. I.; Kim, K.; Park, N. G. Nano-Embossed Hollow Spherical TiO_2 as Bifunctional Material for High-Efficiency Dye-Sensitized Solar Cells. *Adv. Mater.* **2008**, *20*, 195−199.

(9) Mahmoud, M. A.; O'Neil, D.; El-Sayed, M. A. Hollow and Solid Metallic Nanoparticles in Sensing and in Nanocatalysis. *Chem. Mater.* **2014**, *26*, 44−58.

(10) Lee, J.-H. Gas Sensors Using Hierarchical and Hollow Oxide Nanostructures: Overview. *Sens. Actuators, B* **2009**, *140*, 319−336.

(11) Oh, W. K.; Kim, S.; Choi, M.; Kim, C.; Jeong, Y. S.; Cho, B. R.; Hahn, J. S.; Jang, J. Cellular Uptake, Cytotoxicity, and Innate Immune Response of Silica-Titania Hollow Nanoparticles Based on Size and Surface Functionality. *ACS Nano* **2010**, *4*, 5301−5313.

(12) Zhao, L.; Li, J.; Shi, Y.; Wang, S.; Hu, J.; Dong, B.; Lu, H.; Wang, P. Double Light-Scattering Layer Film Based on TiO_2 Hollow Spheres and TiO_2 Nanosheets: Improved Efficiency in Dye-Sensitized Solar Cells. *J. Alloys Compd.* **2013**, *575*, 168−173.

(13) Choi, M.; Kim, C.; Ok Jeon, S.; Soo Yook, K.; Yeob Lee, J.; Jang, J. Synthesis of Titania Embedded Silica Hollow Nanospheres Via Sonication Mediated Etching and Re-Deposition. *Chem. Commun.* **2011**, *47*, 7092−7094.

(14) Yang, Z.; Niu, Z.; Lu, Y.; Hu, Z.; Han, C. C. Templated Synthesis of Inorganic Hollow Spheres with a Tunable Cavity Size onto Core-Shell Gel Particles. *Angew. Chem., Int. Ed.* **2003**, *42*, 1943−1945.

(15) Xu, H.; Wang, W. Template Synthesis of Multishelled Cu_2O Hollow Spheres with a Single-Crystalline Shell Wall. *Angew. Chem., Int. Ed.* **2007**, *46*, 1489−1492.

(16) Deng, D.; Lee, J. Y. Hollow Core-Shell Mesospheres of Crystalline SnO_2 Nanoparticle Aggregates for High Capacity Li^+ Ion Storage. *Chem. Mater.* **2008**, *20*, 1841−1846.

(17) Liang, S.; Yi, J.; Pan, A. Synthesis of Double-Shelled $LiMn_2O_4$ Hollow Microspheres with Enhanced Electrochemical Performance for Lithium Ion Batteries. *Int. J. Electrochem. Sci.* **2013**, *8*, 6535−6543.

(18) Wang, L.; Lou, Z.; Fei, T.; Zhang, T. Zinc Oxide Core−Shell Hollow Microspheres with Multi-Shelled Architecture for Gas Sensor Applications. *J. Mater. Chem.* **2011**, *21*, 19331−19336.

(19) Wu, X.; Lu, G. Q.; Wang, L. Shell-in-Shell TiO_2 Hollow Spheres Synthesized by One-Pot Hydrothermal Method for Dye-Sensitized Solar Cell Application. *Energy Environ. Sci.* **2011**, *4*, 3565−3572.

(20) Stöber, W.; Fink, A.; Bohn, E. Controlled Growth of Monodisperse Silica Spheres in the Micron Size Range. *J. Colloid Interface Sci.* **1968**, *26*, 62−69.

(21) Pattanaik, M.; Bhaumik, S. K. Adsorption Behaviour of Polyvinyl Pyrrolidone on Oxide Surfaces. *Mater. Lett.* **2000**, *44*, 352−360.

(22) Chen, Z. H.; Kim, C.; Zeng, X. B.; Hwang, S. H.; Jang, J.; Ungar, G. Characterizing Size and Porosity of Hollow Nanoparticles: Saxs, Sans, Tem, Dls, and Adsorption Isotherms Compared. *Langmuir* **2012**, *28*, 15350−15361.

(23) Usami, A. Theoretical Simulations of Optical Confinement in Dye-Sensitized Nanocrystalline Solar Cells. *Sol. Energy Mater. Sol. Cells* **2000**, *64*, 73−83.
(24) Ferber, J.; Luther, J. Computer Simulations of Light Scattering and Absorption in Dye-Sensitized Solar Cells. *Sol. Energy Mater. Sol. Cells* **1998**, *54*, 265−275.
(25) Zhang, Q.; Myers, D.; Lan, J.; Jenekhe, S. A.; Cao, G. Applications of Light Scattering in Dye-Sensitized Solar Cells. *Phys. Chem. Chem. Phys.* **2012**, *14*, 14982−14998.
(26) Kondo, Y.; Yoshikawa, H.; Awaga, K.; Murayama, M.; Mori, T.; Sunada, K.; Bandow, S.; Iijima, S. Preparation, Photocatalytic Activities, and Dye-Sensitized Solar-Cell Performance of Submicron-Scale TiO_2 Hollow Spheres. *Langmuir* **2008**, *24*, 547−550.
(27) Qian, J.; Liu, P.; Xiao, Y.; Jiang, Y.; Cao, Y.; Ai, X.; Yang, H. TiO_2-Coated Multilayered SnO_2 Hollow Microspheres for Dye-Sensitized Solar Cells. *Adv. Mater.* **2009**, *21*, 3663−3667.
(28) Johnson, R. W.; Thiele, E. S.; French, R. H. Light-Scattering Efficiency of White Pigments: An Analysis of Model Core−Shell Pigments vs Optimized Rutile TiO_2. *Tappi J.* **1997**, *80*, 233−239.
(29) Wijnhoven, J. E. G. J.; Bechger, L.; Vos, W. L. Fabrication and Characterization of Large Macroporous Photonic Crystals in Titania. *Chem. Mater.* **2001**, *13*, 4486−4499.